

Large decrease of fluctuations for supercooled water in hydrophobic nanoconfinement

Elena G. Strelakova,¹ Marco G. Mazza,² H. Eugene Stanley,¹ and Giancarlo Franzese³

¹*Center for Polymer Studies and Department of Physics,
Boston University, Boston, Massachusetts 02215, USA*

²*Stranski-Laboratorium für Physikalische und Theoretische Chemie,
Technische Universität Berlin, Straße des 17. Juni 135, 10623 Berlin, Germany*

³*Departament de Física Fonamental, Universitat de Barcelona,
Diagonal 647, 08028 Barcelona, Spain*

(Dated: 29 January 2011 — smsf29jan.tex)

Abstract

Using Monte Carlo simulations we study a coarse-grained model of a water layer confined in a fixed disordered matrix of hydrophobic nanoparticles at different particle concentrations c . For $c = 0$ we find a first-order liquid-liquid phase transition (LLPT). For $c > 0$ our simulations are consistent with a LLPT line ending in two critical points at low and high pressure P . For $c = 25\%$ at high P and low temperature T we find a dramatic decrease of compressibility K_T , thermal expansion coefficient α_P , and specific heat C_P . Surprisingly, the effect is present also for c as low as 2.4%. We conclude that even a small presence of nanoscopic hydrophobes can drastically suppress thermodynamic fluctuations, making the detection of the LLPT more difficult.

PACS numbers: 64.70.Ja, 65.20.-w, 66.10.C-

Many recent experiments investigate the behavior of water in confined geometries [1] for its relevance to nanotechnology, e.g., filtering water in carbon nanotubes [2], and biophysics, e.g., intracellular water [3]. An interesting property of nanoconfined water is that it remains liquid at temperatures where bulk water freezes. The present technology allows us to observe bulk water in its liquid phase below 0°C if quenched very rapidly (supercooled), but ice formation cannot be avoided below $T_H = -41^\circ\text{C}$ (at 1 atm). Interestingly, a number of theories and models predict a peculiar thermodynamic behavior for bulk water below T_H , with a liquid-liquid phase transition (LLPT) [4–6]. Although studying nanoconfined water could shed light on the phase diagram of deeply supercooled water, experiments and simulations [7] show that fluid-fluid phase transitions in a confined space can differ from those in bulk water. Several studies using specific geometries, e.g., slits [8–10] or disordered matrices of disks or spheres [11, 12], have clarified some aspects but leave open questions about the thermodynamics of supercooled confined water [1, 9, 13, 14].

It has been proposed that supercooled water forms highly structured regions in the hydration shell of nonpolar solutes [15], where the hydrogen bond (HB) network is weakened only when the size of the hydrophobic particles is above a characteristic value [16], calculated using free energy analysis to be ≈ 1 nm [17]. Muller explained experimental results by assuming enthalpic strengthening of the hydration HBs with a simultaneous entropy increase in the hydration shell [18].

Here, motivated by several experiments on water in a strong hydrophobic confinement [1–3, 19], we consider a water monolayer of thickness $h \lesssim 1$ nm in a volume \mathcal{V} partitioned into \mathcal{N} cells of a square section of size $\sqrt{\mathcal{V}/\mathcal{N}h}$. Each cell is occupied by either a water molecule or a hydrophobic particle. Particles can occupy more than one cell, depending on their size, are spherical and approximated by the set of cells with more than 50% of their volume inaccessible to water. Particles are randomly distributed and form a fixed matrix that mimicks a porous system or a rough atomic interface. $N \leq \mathcal{N}$ is the total number of cells occupied by water molecules and $V \leq \mathcal{V}$ is their total volume. The Hamiltonian for water-water interaction is [5]

$$\mathcal{H} \equiv \sum_{ij} U(r_{ij}) - JN_{\text{HB}} - J_\sigma \sum_i n_i \sum_{(k,\ell)_i} \delta_{\sigma_{ik}, \sigma_{i\ell}}. \quad (1)$$

Here r_{ij} is the distance between water molecules i and j , $U(r) \equiv \infty$ for $r < r_0 \equiv 2.9$ Å, the water van der Waals diameter, $U(r) \equiv \epsilon_w [(r_0/r)^{12} - (r_0/r)^6]$ for $r \geq r_0$ with $\epsilon_w \equiv 5.8$ kJ/mol,

the van der Waals attraction energy, and $U(r) = 0$ for $r > r_c = \sqrt{\mathcal{V}/h}/4$, the cut-off distance.

The second term of Eq. (1) describes the directional HB interaction, with $J \equiv 2.9$ kJ/mol, and the total number of HBs $N_{HB} \equiv \sum_{\langle i,j \rangle} n_i n_j \delta_{\sigma_{ij}, \sigma_{ji}}$, where $n_i \equiv 1$ for a water molecule when $Nv_0/V \geq 0.5$ (liquid density, with $v_0 \equiv hr_0^2$) and $n_i \equiv 0$ for a hydrophobic particle. A HB breaks when the OH—O distance exceeds $r_{\max} - r_{\text{OH}} = 3.14\text{\AA}$, because $n_i n_j = 0$ when the O—O distance $r \geq r_{\max} \equiv r_0\sqrt{2} = 4.10\text{\AA}$ ($r_{\text{OH}} = 0.96\text{\AA}$). It also breaks if $\widehat{\text{OOH}} > 30^\circ$. Therefore, only 1/6 of the orientation range $[0, 360^\circ]$ in the OH—O plane is associated with a bonded state. By allowing $q = 6$ possible states for each index σ_{ij} , we account for the entropy loss associated with the formation of a HB because, by definition, $\delta_{\sigma_{ij}, \sigma_{ji}} \equiv 1$ if $\sigma_{ij} = \sigma_{ji}$, $\delta_{\sigma_{ij}, \sigma_{ji}} \equiv 0$ otherwise. The notation $\langle i, j \rangle$ denotes that the sum is performed over nearest-neighbors (n.n.) water molecules i and j , so that each water molecule can form up to four HBs.

HB formation increases the volume per molecule, because it leads to an open network of molecules with reduced n.n. due to close molecular packing. We incorporate this effect by an enthalpy increase Pv_{HB} for each HB, where $v_{\text{HB}}/v_0 = 0.5$ is the average density increase between high density ices VI and VIII and low density (tetrahedral) ice Ih.

The third term of Eq. (1) accounts for the HB cooperativity, with $J_\sigma \equiv 0.29$ kJ/mol, where $(k, \ell)_i$ indicates each of the six different pairs of the four bond-indices σ_{ij} of a molecule i . It gives rise to the O—O—O correlation, locally driving the molecules toward an ordered configuration [14].

The water-nanoparticle interaction is purely repulsive, $U_{\text{wn}}(r) \equiv \epsilon_h[(r_0/r)^{12}]$, with $\epsilon_h \equiv \epsilon_w\sqrt{0.1} = 1.8$ kJ/mol [12], where $r < r_c$ is the distance between the water cell and each of the cells occupied by the nanoparticle. The restructuring effect of hydrophobic particles on water is incorporated by replacing J and J_σ in the hydration shell with $J^{\text{h}} = 1.30J$ and $J_\sigma^{\text{h}} = 1.30J_\sigma$, following [20]. Because bonding indices facing the nanoparticle cannot form HBs, at intermediate T they have a number of accessible states larger than those facing water molecules, inducing an increase of hydration entropy [18].

We perform Monte Carlo (MC) simulations for constant pressure P , T , and N , with variable water volume $V \equiv V_0 + N_{\text{HB}}v_{\text{HB}}$, where $V_0 \geq Nv_0$ is a stochastic continuous variable that fluctuates following the MC acceptance rule [21]. We simulate systems with $\mathcal{N} \leq 1.6 \times 10^5$ within a fixed matrix of spherical nanoparticles of radius $R = 1.6$ nm, with

nanoparticle concentration $c \equiv (\mathcal{N} - N)/\mathcal{N} = 2.4\%$ and 25% . We repeat the analysis for $R = 0.4$ nm. For $c = 0$, the model has a phase diagram with a first-order LLPT, between a low density liquid and a high density liquid, starting at $P \simeq 0.2$ GPa for $T \rightarrow 0$ and ending in a critical point at $T \simeq 174$ K and $P \simeq 0.13$ GPa [5].

We find that for $c > 0$ the liquid-gas spinodal is shifted to lower T and the line of temperature of maximum density (TMD) is shifted to lower T at low P and to higher T at high P , with respect to the $c = 0$ case, reminiscent of results for other models of confined water [10, 12]. We find stronger changes for increasing c (Fig. 1).

Further, we next find that confinement drastically reduces volume and entropy fluctuations at low T . To quantify this reduction, we calculate volume fluctuations, entropy fluctuations, and cross-fluctuations of volume and entropy, and analyze the associated measurable response function, respectively, isothermal compressibility K_T , isobaric specific heat C_P and isobaric thermal expansion coefficient α_P , e.g., see Figs. (2) and (3). For a water monolayer with $\mathcal{N} = 1.6 \times 10^5$ cells confined within nanoparticles with $R = 1.6$ nm at $c = 25\%$, we find a maximum K_T^{\max} along the isobar at $P \simeq 0.16$ GPa that is 99.7% smaller than the $c = 0$ case. If we decrease c to 2.4%, the reduction of K_T^{\max} is still remarkable: 92.3% (Fig. 3). We find similar reductions for C_P^{\max} and α_P^{\max} .

Such a dramatic reduction of K_T^{\max} at low T and high P suggests a possible change in the region of the phase diagram where water at $c = 0$ displays the LLPT. From the general theory of finite size scaling, we know that at a first-order phase transition K_T^{\max} , C_P^{\max} and α_P^{\max} increase linearly with the number of degrees of freedom, here equal to $4N$. We find a linear increase for $0.14 \text{ GPa} \leq P \leq 0.20 \text{ GPa}$ at $c = 0$, and only for $0.14 \text{ GPa} \leq P < 0.16 \text{ GPa}$ at $c = 25\%$ and 2.4% , consistent with the absence of a first-order LLPT outside these ranges.

To better understand this new feature, i.e., the effect of confinement on the LLPT at high P , we study the finite size scaling of the Binder cumulant [23] $U_{\mathcal{N}} \equiv 1 - [\langle V^4 \rangle_{\mathcal{N}} / 3 \langle V^2 \rangle_{\mathcal{N}}^2]$, where $\langle \cdot \rangle_{\mathcal{N}}$ stands for the thermodynamic average for a system with \mathcal{N} cells. For $\mathcal{N} \rightarrow \infty$, at fixed c and P , $U_{\mathcal{N}} = 2/3$ for any T away from a first-order phase transition, while $U_{\mathcal{N}}^{\min} < 2/3$ at a first-order phase transition [23].

For $c = 0$, we find that $U_{\mathcal{N}}^{\min} < 2/3$ for $\mathcal{N} \rightarrow \infty$ at $0.14 \text{ GPa} \leq P \leq 0.20 \text{ GPa}$, while $U_{\mathcal{N}}^{\min} = 2/3$, within the error bar, at $P = 0.12 \text{ GPa}$ (Fig. 4a). Hence, this analysis confirms that for $c = 0$ there is a first-order LLPT in the range $0.14 \text{ GPa} \leq P \leq 0.2 \text{ GPa}$.

For $c = 2.4\%$ and 25% , we find that, for large \mathcal{N} , $U_{\mathcal{N}}^{\min} < 2/3$ at 0.14 GPa, but not at 0.12 GPa or at $P \geq 0.16$ GPa (Fig. 4b,c). Hence, for $c = 2.4\%$ and 25% the first-order LLPT occurs only in a limited range of pressures around 0.14 GPa, consistent with our results for $\langle \delta V^2 \rangle$ (Fig. 2) or K_T^{\max} (Fig. 3), with two end-points: one at ≈ 0.15 GPa, another at ≈ 0.13 GPa (Fig. 1).

We interpret our findings as follows. As a consequence of the stronger HB in the hydration shell of each solute, at low T the hydration water is more ordered with respect to the $c = 0$ case. However, shells around different nanoparticles have a different local orientational order. This generates competing domains, reminiscent of the locally structured regions proposed in Ref. [15], and exhibits no macroscopic order (upper inset in Fig. 1). The large decrease in fluctuations and response functions, such as K_T , is due to the presence of many domain boundaries. Our results for c as low as 2.4% indicates that the decrease is due to the introduction of a characteristic length scale, inversely proportional to c , that limits the growth of the ordered structured regions. This is consistent also with the results for K_T^{\max} (Fig. 3), where the lower is c , the larger is N beyond which the confined behavior deviates from the $c = 0$ case.

In previous theoretical analyses, with water confined by a fixed matrix of randomly distributed Lennard-Jones disks, the reduction of compressibility was observed only for large hydrophobic obstacle concentrations [11]. Here, instead, we find that K_T is reduced for very low c .

Our results are qualitatively consistent with recent experiments on H_2O confined in the hydrophobic mesoporous material CMK-1-14 consisting of micrometer-sized grains, each with a 3-dimensional interconnected bicontinuous pore structure, with an average pore diameter 14 \AA , at a hydration level of 99% at ambient pressure [19]. Zhang et al. find that the TMD is shifted down by 17 K with respect to the hydrophilic confinement in silica mesopores and that α_P shows a much broader peak, spanning from 240 to 180 K , in contrast to the sharp peak at 230 K in hydrophilic confinement [19], reminiscent of our results on the shift of TMD and the reduction of the response functions with respect to the $c = 0$ case.

Recent results for small angle x-ray scattering for aqueous solutions of amphiphilic tetraalkyl-ammonium cations at ambient conditions suggest that the strengthening of the structure of hydration water is present only for solutes with radius smaller than $\approx 0.44 \text{ nm}$ [24]. We therefore repeat our analysis for small nanoparticles with $R = 0.4 \text{ nm}$, and find

that our results are robust if the amount of hydrophobic interface in contact with water is kept constant with respect to the case of $R = 1.6$ nm.

In conclusion, we predict that a water monolayer confined in a fixed matrix of hydrophobic nanoparticles at concentration c displays changes in the thermodynamics and a drastic reduction, $> 90\%$, in K_T , C_P , and α_P with respect to the $c = 0$ case. At c as small as 2.4% the first-order LLPT at high P is no longer detected.

We thank S. V. Buldyrev, P. Ch. Ivanov, and K. Stokely for discussions and acknowledge support by NSF grants CHE0908218 and CHE0911389. GF thanks the Spanish MICINN grant FIS2009-10210 (co-financed FEDER).

-
- [1] M.-C. Bellissent-Funel et al., Phys. Rev. E **51**, 4558 (1995). J. Swenson et al., Phys. Rev. Lett., **96**, 247802 (2006). F. Mallamace et al., J. Chem. Phys. **124**, 161102 (2006). S.-H. Chen et al., Proc. Natl. Acad. Sci. U.S.A. **103**, 12974 (2006). D. Liu et al. *ibid.* **104**, 9570 (2007). G. Findenegg et al., ChemPhysChem **9**, 2651 (2008). C. A. Angell, Science **319**, 582 (2008). R. Mancinelli et al., J. Phys. Chem. Lett. **1**, 1277 (2010).
 - [2] M. Majumder et al., Nature **438**, 44 (2005). S. Joseph and N. R. Aluru, Phys. Rev. Lett. **101**, 064502 (2008).
 - [3] S. Granick and S. C. Bae, Science **322**, 1477 (2008).
 - [4] P. H. Poole et al., Nature **360**, 324 (1992).
 - [5] G. Franzese et al., J. Phys.: Condens. Matt. **14**, 2201 (2002); **19**, 205126 (2007); Phys. Rev. E **67**, 011103 (2003). P. Kumar et al., Phys. Rev. Lett. **100**, 105701 (2008). K. Stokely et al., Proc. Natl. Acad. Sci. U.S.A. **107**, 1301 (2010).
 - [6] D. Paschek, J. Chem. Phys. **120**, 10605 (2004).
 - [7] R. Kurita and H. Tanaka, Phys. Rev. Lett. **98**, 235701 (2007). P. G. De Sanctis Lucentini and G. Pellicane, *ibid.* **101**, 246101 (2008).
 - [8] K. Koga et al., Nature **408**, 564 (2000). N. Giovambattista et al., Proc. Natl. Acad. Sci. U.S.A. **105**, 2274 (2008); G. Franzese and F. de los Santos, J. Phys.: Condens. Matter **21**, 504107 (2009).
 - [9] T. M. Truskett et al., J. Chem. Phys. **114**, 2401 (2001).
 - [10] P. Kumar et al., Phys. Rev. E **72**, 051503 (2005).

- [11] T. Urbic et al., J. Mol. Liq. **112**, 71 (2004).
- [12] P. Gallo and M. Rovere, Phys. Rev. E **76**, 061202 (2007).
- [13] A. K. Soper, Mol. Phys. **106**, 2053 (2008).
- [14] M. A. Ricci et al., Faraday Discuss. **141**, 347 (2009).
- [15] H. S. Frank and M. W. Evans, J. Chem. Phys. **13**, 507 (1945). K. A. T. Silverstein et al., *ibid.* **111**, 8000 (1999).
- [16] F. H. Stillinger, J. Solution. Chem. **2**, 141 (1973).
- [17] D. Chandler, Nature **437**, 640 (2005).
- [18] N. Muller, Acc. Chem. Res. **23**, 23 (1990).
- [19] Y. Zhang et al., J. Phys. Chem. B **113**, 5007 (2009).
- [20] B. Patel et al., Biophys.J. **93**, 4116 (2007).
- [21] M. G. Mazza et al., Comp. Phys. Comm. **180**, 497 (2009).
- [22] At $c = 0$, K_T^{\max} increases for higher P because $\langle \delta V^2 \rangle$ depends weakly on P , and K_T^{\max} occurs at lower $T\langle V \rangle$.
- [23] K. Binder, Phys. Rev. Lett. **47** 693 (1981); G. Franzese and A. Coniglio, Phys. Rev. E **58**, 2753 (1998).
- [24] N. Huang et al., J. Chem. Phys. (under review).

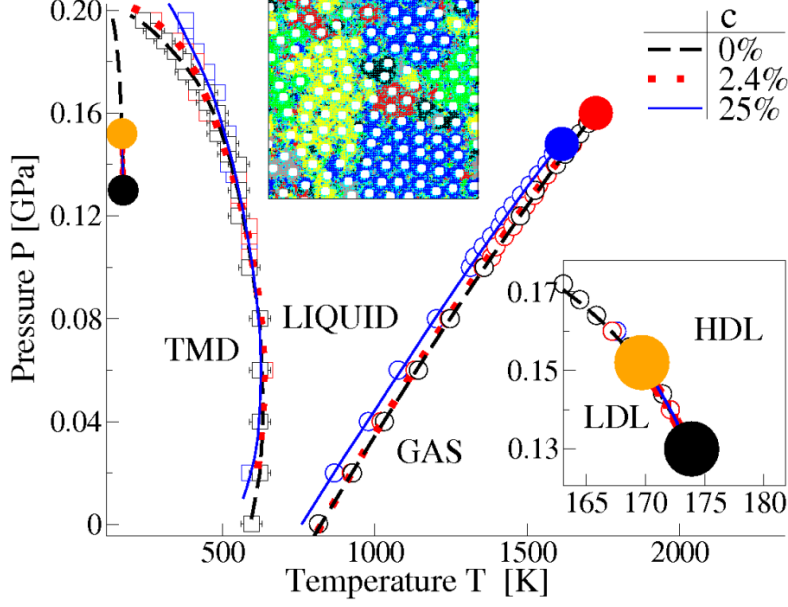


FIG. 1: P - T phase diagram for different nanoparticle concentrations c . Open circles estimate liquid-to-gas spinodal line, squares estimate TMD line. In this and all other figures, where not shown, errors are smaller than the symbol size. Lines are guides for the eyes (dashed for $c = 0$, dotted for 2.4%, full for 25%). Critical points are shown as large full circles. The liquid-gas critical point is the same for $c = 0$ and 2.4%, while occurs at lower P and T for $c = 25\%$. Lower inset: enlarged view of the low- T region. The first-order LLPT ends in a critical point at $T \simeq 174$ K and $P \simeq 0.13$ GPa for all c . At $c = 2.4\%$ and 25% at $P > 0.15$ GPa the first-order LLPT is no longer detected, indicating a new high- P critical point. Upper inset: configuration at $T \simeq 160$ K and $P = 0.18$ GPa for $c = 25\%$. Hydrophobic nanoparticles are in white; HBs are in different colors for different ordered domains.

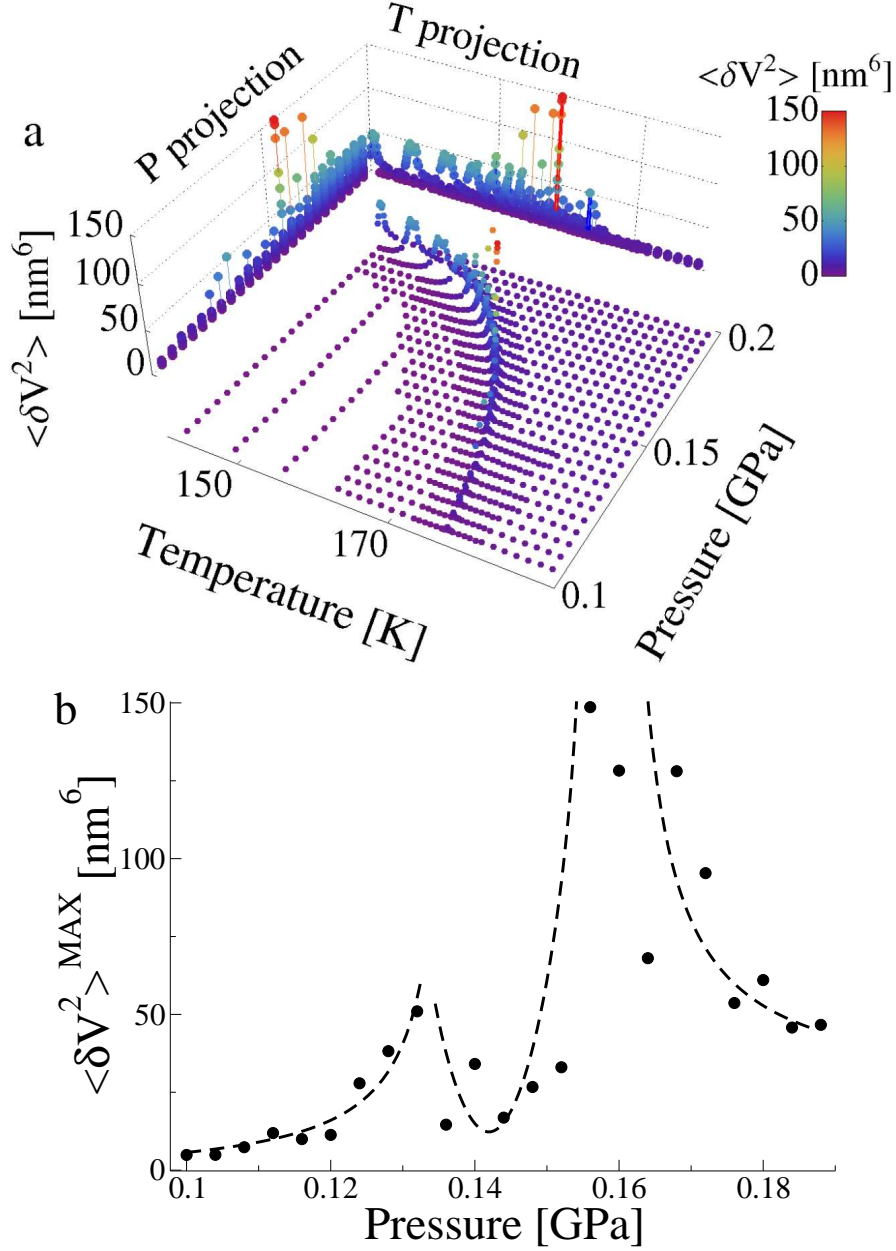


FIG. 2: (a) Volume fluctuations $\langle \delta V^2 \rangle$ for $c = 25\%$ and $\mathcal{N} = 10^4$ have maxima that follow a locus in the $P - T$ plane that does not change, within the error bars, with c or \mathcal{N} . The projections $\langle \delta V^2 \rangle$ vs P or vs T clarify that the maxima do not change monotonically with P or T . (b) The projection of maxima of $\langle \delta V^2 \rangle$ increase approaching $P = 0.132$ GPa and 0.156 GPa, consistent with our estimate of two critical points at ≈ 0.13 GPa and ≈ 0.15 GPa. Dashed lines are guides for the eyes.

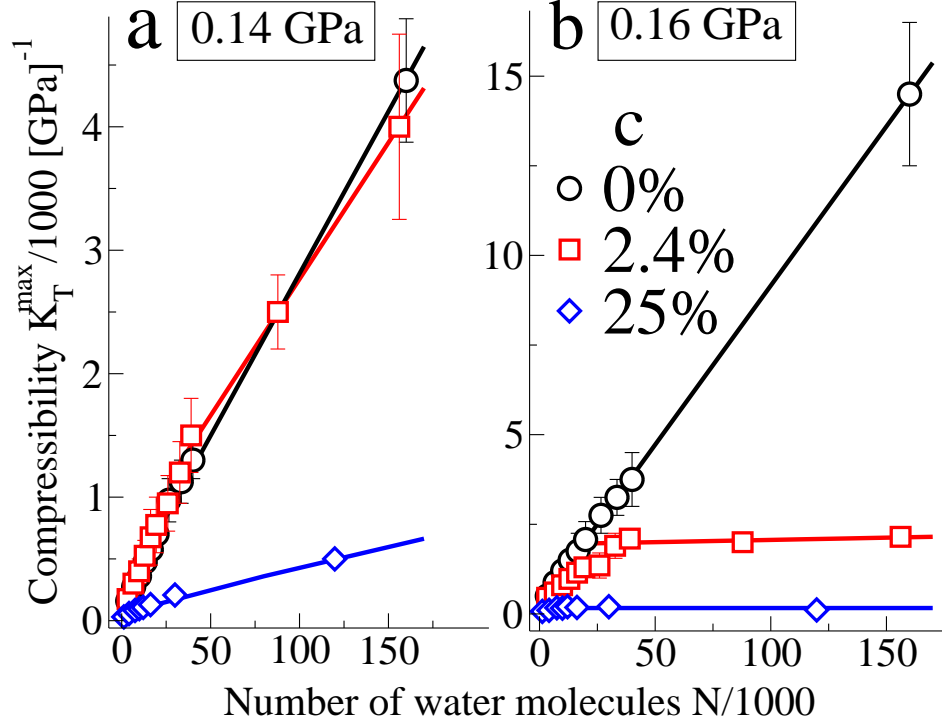


FIG. 3: Maxima K_T^{\max} of the isothermal compressibility $K_T \equiv \langle \delta V^2 \rangle / (k_B T \langle V \rangle)$ vs number of water molecules N for $c = 0, 2.4\%$ and 25% . (a) Linear increase in K_T^{\max} with N for $P = 0.14$ GPa, consistent with a first-order LLPT for all c . (b) At $P = 0.16$ GPa, K_T^{\max} increases linearly for $c = 0$ indicating a first-order LLPT, but saturates for $c = 2.4\%$ and 25% , consistent with the absence of a first-order LLPT [22].

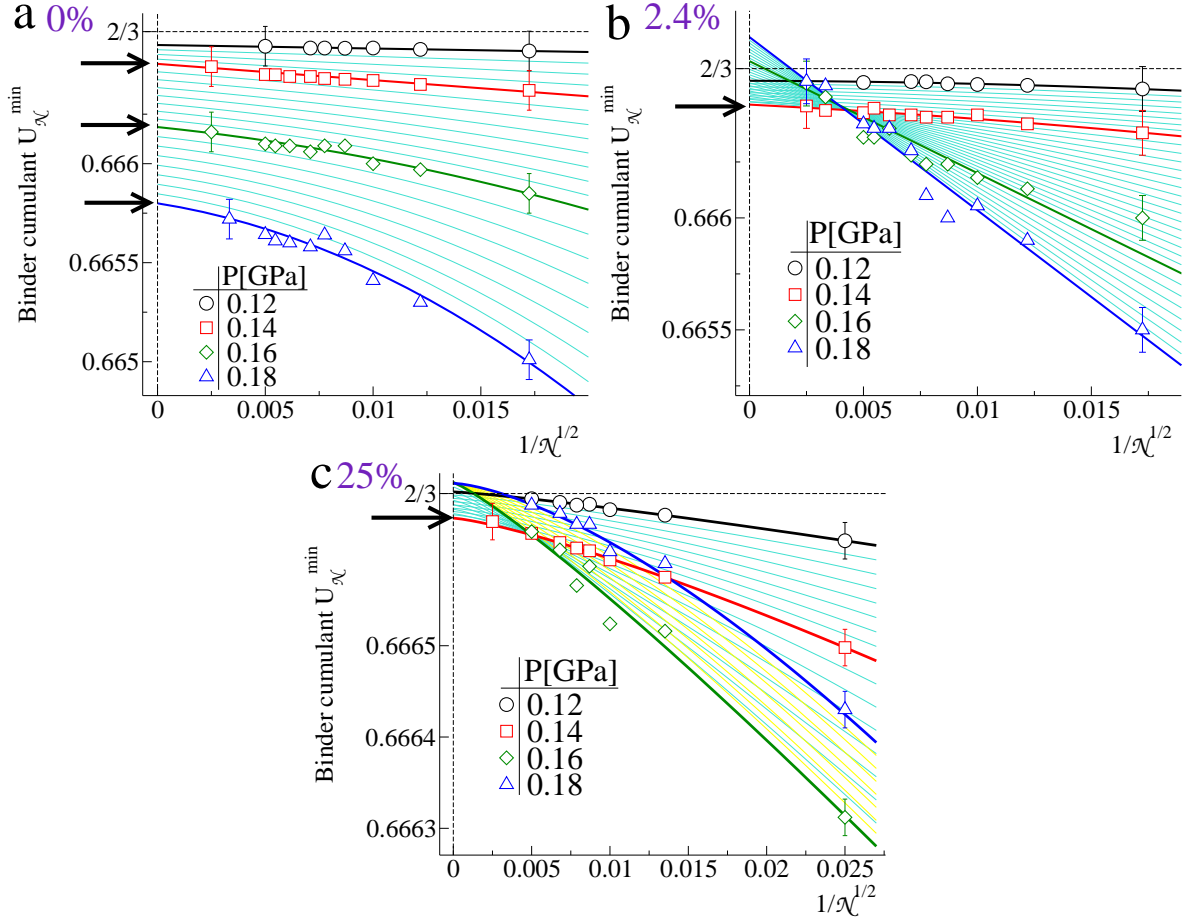


FIG. 4: (a) At $c = 0$, for $\mathcal{N} \rightarrow \infty$ is $U_{\mathcal{N}}^{\min} = 2/3$, within the error bar, for $P = 0.12$ GPa and tends to a value $\leq 2/3$ for $P \geq 0.14$ GPa, indicating a first-order LLPT for $P \geq 0.14$ GPa. At nanoparticle concentrations $c = 2.4\%$ (b) and 25% (c), for $\mathcal{N} \rightarrow \infty$ we find $U_{\mathcal{N}}^{\min} < 2/3$ only for $P = 0.14$ GPa, indicating that the first-order LLPT is washed out by the hydrophobic confinement at high P . For sake of clarity, typical error bars are indicated only for a few points. Lines through the points are fits, while other lines are linear interpolations between fits at intermediate P . Black arrows mark isobars crossing the first-order LLPT line.